Vol 18 No 1, January 2009
1674-1056/2009/18(01)/0136-06

Chinese Physics B

© 2009 Chin. Phys. Soc.
and IOP Publishing Ltd

Nucleon–nucleon interactions in the double folding model for fusion reactions*

Zhang Gao-Long(张高龙)[a)†], Liu Hao(刘 浩)[b)], and Le Xiao-Yun(乐小云)[a)]

[a)] *Department of Physics, School of Science, Beijing University of Aeronautics and Astronautics, Beijing* 100083, *China*

[b)] *Physics Laboratory, Lanzhou Commercial College, Lanzhou* 730020, *China*

(Received 19 April 2008; revised manuscript received 27 August 2008)

Nucleus–nucleus potentials are determined in the framework of double folding model for M3Y–Reid and M3Y–Paris effective nucleon–nucleon (NN) interactions. Both zero-range and finite-range exchange parts of NN interactions are considered in the folding procedure. In this paper the spherical projectile–spherical target system ^{16}O+^{208}Pb is selected for calculating the barrier energies, fusion cross sections and barrier distributions with the density-independent and density-dependent NN interactions on the basis of M3Y–Reid and M3Y–Paris NN interactions. The barrier energies become lower for Paris NN interactions in comparison with Reid NN interactions, and also for finite-range exchange part in comparison with zero-range exchange part. The density-dependent NN interactions give similar fusion cross sections and barrier distributions, and the density-independent NN interaction causes the barrier distribution moving to a higher position. However, the density-independent Reid NN interaction with zero-range exchange part gives the lowest fusion cross sections. We find that the calculated fusion cross sections and the barrier distributions are in agreement with the experimental data after renormalization of the nuclear potential due to coupled-channel effect.

Keywords: nucleon–nucleon interaction, double folding model, fusion
PACC: 2500, 2570

In many nuclear reaction processes the nucleus–nucleus potential is one of the important quantities, for example in elastic scattering of α-nucleus and light heavy-ion (HI) systems,[1−4] in particular for the simple one-dimensional barrier penetration model (1D BPM) of fusion reaction, the barrier energy, radius and curvature can be determined by nuclear potential and Coulomb potential. Since the Coulomb potential can be calculated accurately, the remaining work is to calculate the nuclear potential. Many HI systems may be understood in terms of empirical parametrizations of nuclear potential. Usually phenomenological Woods–Saxon forms are used for both the real and imaginary parts of the optical potential. However, it is desirable to relate the nucleus–nucleus nuclear interaction to the nucleon–nucleon nuclear interaction. The nuclear potential may be obtained by integrating a nucleon–nucleon interaction over the matter distributions of the two colliding nuclei. This approach is called the folding model. It produces the dominant part of the real optical potential for nuclear reactions (elastic scattering, fusion reaction), proton-decay of proton emitter, α-decay half-lives of superheavy nuclei and complex cluster emission (^{14}C–^{34}Si) of heavy nuclei. Among various models of HI systems, the double folding model has been widely and successfully used to generate the real part of HI optical potential.[5−7] This model gives the leading term in the expression of the optical potential.

The basic input into folding calculation is the nuclear densities of the colliding nuclei and the effective nucleon–nucleon (NN) interaction. Though the densities can be accurately determined from the nuclear models or electron scattering data, it is still necessary to have a realistic effective NN interaction in the calculation of double folding model. In this paper, the effective NN interactions are divided into density-independent and density-dependent NN interactions on the basis of M3Y–Reid and M3Y–Paris NN interactions, with their exchange parts divided into zero-range and finite-range interactions. For reaction systems, the interacting nuclei generally have a ground-state matter density distribution which is spherically symmetric. In the present paper, we limit ourselves to the fusion reaction involving spherical projectile and spherical target nuclei. The barrier energy, radius and

*Project supported by the National Natural Science Foundation of China (Grant No 60572177).
†E-mail: zgl@buaa.edu.cn

curvature of the ^{16}O+^{208}Pb system are known by using the different NN interactions, thus the fusion excitation functions can be obtained and the theoretical barrier distributions extracted. We compare the behaviours of the different NN interactions, the results of fusion excitation functions and barrier distributions with the experimental data of the ^{16}O+^{208}Pb system in order to find the differences in the calculated results of fusion reactions. Finally, we employ the renormalization factor in fusion reactions in the double folding model by considering the coupled-channel effect.

In the double folding model, the real part of nuclear potential is written as

$$V_{\rm N}(r) = \int\int \rho_{\rm p}(\boldsymbol{r}_1) v(\boldsymbol{s} = |\boldsymbol{R}+\boldsymbol{r}_2-\boldsymbol{r}_1|)\rho_{\rm T}(\boldsymbol{r}_2){\rm d}\boldsymbol{r}_1{\rm d}\boldsymbol{r}_2, \tag{1}$$

where v is the NN interaction between two nucleons, $\rho_{\rm p}(r_1)$ and $\rho_{\rm T}(r_2)$ are the matter density distributions of the projectile (P) and target (T) nuclear ground states, respectively, which are normalized as

$$\int \rho_i(\boldsymbol{r}_i){\rm d}\boldsymbol{r}_i = A_i. \tag{2}$$

In this paper the matter densities of the colliding nuclei are denoted as two-parameter Fermi distribution $\rho(r) = \rho_0/[1+\exp((r-c)/a)]$ with parameters obtained from electron scattering data.[8] Now the optical potential of halo nuclei attracts much attention. The matter density of halo nuclei also enters into this model, which can be found in Ref.[5]. The vector $\boldsymbol{s} = \boldsymbol{R} + \boldsymbol{r}_2 - \boldsymbol{r}_1$ corresponds to the distance between two specified interacting points of the projectile and target, whose radius vectors are $\boldsymbol{r}_1$ and $\boldsymbol{r}_2$, respectively. $\boldsymbol{R}$ denotes the vector between the centre of mass of the two nuclei. The detailed description of this model can be found also in Ref.[5]. In order to make this paper self-consistent, we present the principal formulas of NN interactions in the following.

For NN interactions, the popular choices have frequently been based on the M3Y interactions which were designed to reproduce the $\boldsymbol{G}$-matrix elements of Reid[9] and Paris[10] NN interactions in an oscillator basis. We refer to these as M3Y–Reid and M3Y–Paris interactions, respectively. Explicit forms are given below.

The direct parts are
M3Y–Reid:

$$v_{\rm D}(r) = \left[7999\frac{{\rm e}^{-4r}}{4r} - 2134\frac{{\rm e}^{-2.5r}}{2.5r}\right]{\rm MeV}, \tag{3}$$

M3Y–Paris:

$$v_{\rm D}(r) = \left[11062\frac{{\rm e}^{-4r}}{4r} - 2538\frac{{\rm e}^{-2.5r}}{2.5r}\right]{\rm MeV}, \tag{4}$$

and the knock-on exchange parts in the finite-range exchanges are
M3Y–Reid:

$$v_{\rm EX}(r) = \left[4631\frac{{\rm e}^{-4r}}{4r} - 1787\frac{{\rm e}^{-2.5r}}{2.5r} - 7.847\frac{{\rm e}^{-0.7072r}}{0.7072r}\right]{\rm MeV}, \tag{5}$$

M3Y–Paris:

$$v_{\rm EX}(r) = \left[-1524\frac{{\rm e}^{-4r}}{4r} - 518.8\frac{{\rm e}^{-2.5r}}{2.5r} - 7.847\frac{{\rm e}^{-0.7072r}}{0.7072r}\right]{\rm MeV}. \tag{6}$$

However, many other calculations use the zero-range pseudo-potential to represent the knock-on exchange. The results can be expressed as
M3Y–Reid:

$$\hat{J}(E) \approx -276[1-0.005(E/A)]{\rm MeV}\cdot{\rm fm}^3, \tag{7}$$

M3Y–Paris:

$$\hat{J}(E) \approx -590[1-0.002(E/A)]{\rm MeV}\cdot{\rm fm}^3, \tag{8}$$

where E/A is the bombarding energy per projectile nucleon in MeV. These density-independent M3Y interactions have been successfully used in the folding model of the HI optical potential at relatively low energy in earlier work.[11] However, in the case of refractive nuclear scattering, characterized by the observation of 'rainbow' features, which were observed first for α particles and later for other light HI systems,[1–4] the simple M3Y interactions failed to give a good description of the data. At the same time, a nuclear matter study within the Hartree–Fock (HF) frame has shown[12] that the original density-independent NN interactions failed to have the saturation in cold nuclear matter, so leading to collapse. This has motivated the inclusion of an explicit density-dependent force in the original M3Y interactions in order to allow saturation to occur. A multiplier $F(\rho)$ enters into the density-independent NN interactions, whose exchange parts are the finite-range interactions in Eqs.(5) and (6), which are considered as anti-symmetrization of the system. The function F is written as

$$F(\rho) = C[1+\alpha\exp(-\beta\rho) - \gamma\rho]. \tag{9}$$

So the direct parts of Eqs.(3) and (4), and exchange parts of Eqs.(5) and (6) can be replaced by the

density-dependent forces. In the course of these applications to scattering data, it is necessary to introduce an additional energy dependent factor over that provided by localizing the exchange potential.[12] This is parametrized as a linear function

$$g(E) = [1 - k(E/A)] \tag{10}$$

with k=0.002MeV^{-1} for Reid interaction or k=0.003MeV^{-1} for Paris interaction. The full interaction form is expressed as

$$v_{\mathrm{D(EX)}}(\rho, r) = g(E)F(\rho)v_{\mathrm{D(EX)}}(r). \tag{11}$$

In this paper, the density-dependent NN interactions are DDM3Y1, BDM3Y1 and CDM3Y(1–6) according to the different parameters C, α, β and γ, which are given in Table 1. These interactions give the same saturation values (a saturation density of about 0.17 fm^{-3} and a binding energy per nucleon of about 16 MeV) except DDM3Y1 which gives the wrong density (0.07 fm^{-3}). They result in different values of the nuclear incompressibility K_0, which is related to the different curvature of the binding energy near the saturation point although the different density-dependent NN interactions give the same saturation properties. Their incompressibility values are shown in Table 1. In order to compare easily, we denote the zero-range and finite-range exchange parts of the density-independent, DDM3Y1, CDM3Y(1–6) and BDM3Y1 by the labels 0–9 one by one. In Table 1 2R and 2P represent M3Y–Reid and M3Y–Paris types for the direct parts and the exchange parts in DDM3Y1, respectively; while 9R and 9P in BDM3Y1 are similar to 2R and 2P in DDM3Y1, respectively.

Table 1. The coefficients of the different density-dependent NN interactions taken from Refs.[13] and [14].

label	interaction	C	α	β	γ	K_0
0(zero)	independent	1.0	0.0	0.0	0.0	
1(finite)	independent	1.0	0.0	0.0	0.0	
2R	DDM3Y1(Reid)	0.2843	3.6391	2.9605	0.0	171
2P	DDM3Y1(Paris)	0.2963	3.7231	3.7384	0.0	176
3	CDM3Y1	0.3429	3.0232	3.5512	0.5	188
4	CDM3Y2	0.3346	3.0357	3.0685	1.0	204
5	CDM3Y3	0.2985	3.4528	2.6388	1.5	217
6	CDM3Y4	0.3052	3.2998	2.3180	2.0	228
7	CDM3Y5	0.2728	3.7367	1.8294	3.0	241
8	CDM3Y6	0.2658	3.8033	1.4099	4.0	252
9R	BDM3Y1(Reid)	1.2253	0.0	0.0	1.5124	232
9P	BDM3Y1(Paris)	1.2521	0.0	0.0	1.7452	270

According to Ref.[15], the different models for the Coulomb potential provide very similar results in the region of the barrier radius for a spherically symmetric reaction system. Here, we choose the conventional point-like plus uniform charge model to calculate the Coulomb potential,

$$V_{\mathrm{C}}(R) = Z_{\mathrm{P}}Z_{\mathrm{T}}e^2 \begin{cases} \dfrac{1}{R}, & (R > R_{\mathrm{C}}), \\ \dfrac{1}{2R_{\mathrm{C}}}\left[3 - \left(\dfrac{R}{R_{\mathrm{C}}}\right)^2\right], & (R < R_{\mathrm{C}}) \end{cases} \tag{12}$$

with e^2=1.44MeV·fm, $R_{\mathrm{C}} = R_{\mathrm{P}} + R_{\mathrm{T}}$, $R_i = 1.76Z_i^{1/3} - 0.96$ fm, here i=P, T.

The total nucleus–nucleus potential V is composed of nuclear potential V_{N} and Coulomb potential V_{C} for a spherically symmetric system,

$$V = V_{\mathrm{N}} + V_{\mathrm{C}}. \tag{13}$$

In the fusion reaction, the transmission coefficient can be calculated using Wentzel–Kramers–Brillouin (WKB) approximation[16] for penetration through the barrier. Under such an approximation, one obtains a closed form expression for σ_{fus} given by[17]

$$\sigma_{\mathrm{fus}} = \frac{\hbar\omega R_{\mathrm{B}}^2}{2E_{\mathrm{cm}}} \ln\left[1 + \exp\left(\frac{2\pi}{\hbar\omega}(E_{\mathrm{cm}} - V_{\mathrm{B}})\right)\right], \tag{14}$$

where V_{B} and R_{B} denote the barrier energy and radius, respectively. The barrier curvature is calculated with

$$\hbar\omega = \left|\frac{\hbar^2}{2\mu}\frac{\mathrm{d}^2V}{\mathrm{d}r^2}\right|, \tag{15}$$

where μ is the reduced mass of the system.

Using the above formulas, we calculate the nucleus–nucleus interaction potentials with the different NN interactions and Coulomb potential of the ^{16}O+^{208}Pb system. The barrier energies, radii and curvatures are obtained as shown in Fig.1. It is shown that the calculated barrier energies are higher than the experimental ones, moreover, the barrier energies for Reid interactions are higher than those for Paris interactions, especially that for zero-range exchange part in density-independent Reid interactions is the highest. Changing from zero- to finite-range exchange part reduces the barrier energy. Indeed, the finite-range exchange part is more attractive than zero-range exchange part in both M3Y–Reid and M3Y–Paris interactions. The barrier radii for not only M3Y–Reid type interactions but also M3Y–Paris type interactions are similar; meanwhile, the barrier radii for the density-dependent interactions are larger than those for the density-independent interactions, in which the barrier radius for finite-range exchange part is larger than that for zero-range exchange part. The barrier curvatures are similar for finite-range exchange in density-independent and density-dependent NN interactions between M3Y–Reid and M3Y–Paris types, but there is a difference (about 0.22 MeV) in zero-range exchange between density-independent M3Y–Reid and M3Y–Paris interactions. The curvature of finite-range exchange in density-independent interactions is the largest among all the curvatures of NN interactions.

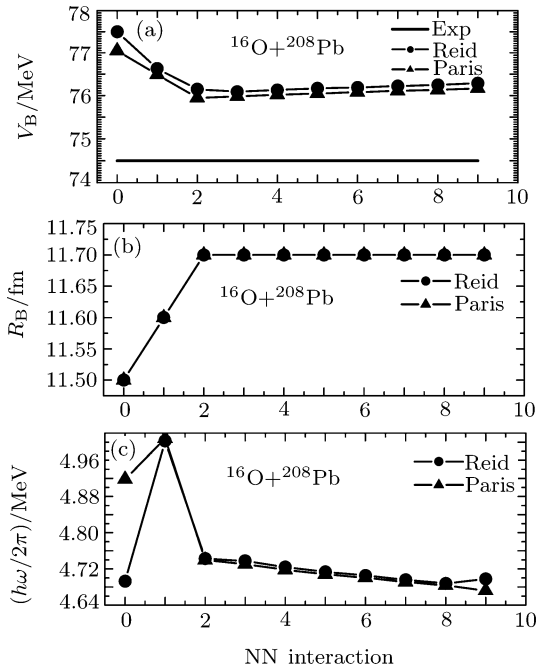


Fig.1. The calculated results for the ^{16}O+^{208}Pb system with different NN interactions on the basis of M3Y–Reid (full circle) and M3Y–Paris (solid triangle) interactions. (a) the calculated barrier energies. The horizontal line indicates the experimental barrier energy of the system; (b) the calculated barrier radii; (c) the calculated barrier curvatures.

In order to understand the above phenomena, we compare the factor F in Eq.(9), which is dependent on the nucleon density and the density overlap at the fusion barrier, with those in the different NN interactions in Fig.2. In Fig.2(a), one sees that the density dependence of Eq.(9) generally reduces the NN interaction near and above the nuclear saturation density. In the region of small density (about less than 0.1 fm^{-3}) the density-dependent NN interactions are enhanced due to F >1 compared with the density-independent NN interactions; moreover, the factors F of DDM3Y1(Paris) and BDM3Y1(Reid) are respectively the largest and the smallest, and those of CDM3Y(1–6) become lower and lower, and thus the barrier energies are sequentially lowered according to the sequence of DDM3Y1(Paris), CDM3Y(1–6) and BDM3Y1(Reid). In Fig.2(b) is shown the typical minimum density in the region of density overlap at the fusion barrier, that is not more than 0.04 fm^{-3} for M3Y zero-range NN interactions, which give the minimum barrier radius about 11.5 fm as shown in Fig.1. After the barrier radius has been changed to about 11.7 fm, the value of the density overlap reduces not more than 0.02 fm^{-3}. The smaller the barrier radius the larger the density overlap and thus the higher the barrier energy, and vice versa. Alike behaviour is shown in Fig.1, in which the density-dependent NN interactions give the larger barrier radii than the density-independent NN interactions, and hence the barrier radius for zero-range exchange part is smaller than that for the finite-range exchange part. And the density-dependent interactions give the lower barrier energies than the density-independent interactions, in which the zero range exchange part shows the higher barrier energy than the finite-range exchange part.

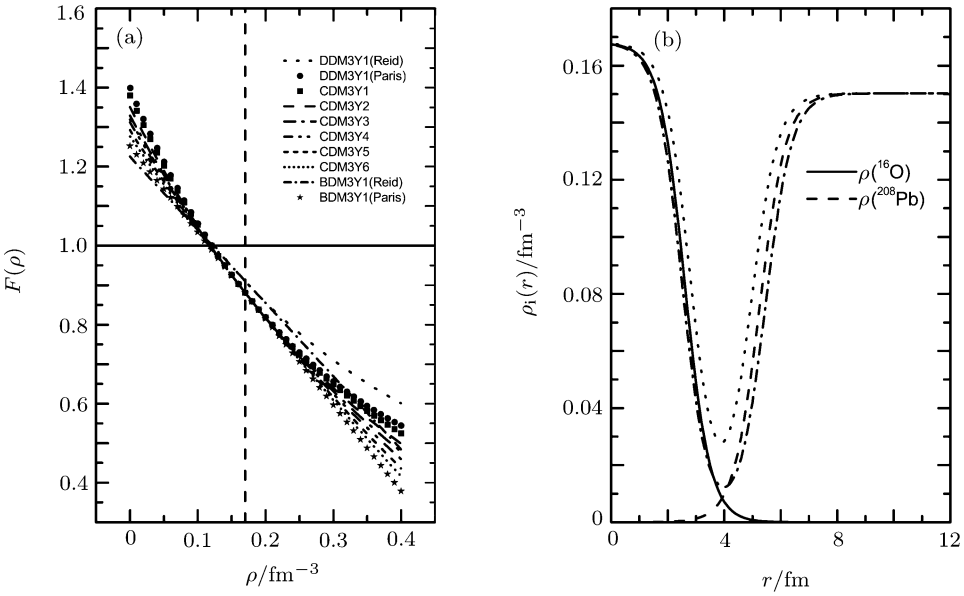


Fig.2. (a) The dependence of factors F in Eq.(9) on the nucleon density. The different symbols denote the different NN interactions shown in Table 1. The horizontal line represents the density-independent forces, and the vertical dash line shows the nuclear saturation density (ρ_0=0.17 fm^{-3}). (b) The density overlap at the fusion barrier. The matter density distribution of ^{16}O is shown by solid line and that of ^{208}Pb by dashed line, and the other lines represent the density overlap of zero-range NN interaction (dotted) at the fusion barrier radius about 11.5fm and that of finite-range NN interaction (dot-dashed) at the fusion barrier radius about 11.7 fm.

By using Eq.(14), the fusion excitation functions of the ^{16}O+^{208}Pb system are obtained with the calculated barrier energies, radii and curvatures for the different types of NN interactions. In Fig.3, it is indicated that at energies near and below the Coulomb barrier the M3Y–Reid NN interaction with zero-range exchange part gives the smallest fusion cross section among all the NN interactions; the fusion cross sections for M3Y–Paris NN interaction with zero-range exchange part are much larger than those for M3Y–Reid NN interaction with zero-range exchange part in the density-independent NN interactions, but they are a little smaller than those for the density-dependent NN interactions. The fusion cross sections are similar for finite-range exchange part in the density-independent and the density-dependent NN interactions. The average fusion barrier energy for the ^{16}O+^{208}Pb reaction is 74.5 MeV, determined empirically from a fit with a single-barrier calculation to the above-barrier fusion cross sections.[18] In the microscopic optical model, the dynamic polarization potential (DPP) resulting from coupling to excited states has been considered. The DPP is closely related to the potential renormalization that is found in the coupled-channel calculation. In Fig.1, it is clearly shown that the fusion barriers calculated based on the double folding model, named uncoupled fusion barriers, lie about 1.5–3 MeV above the empirical fusion barrier. When the potential renormalization is taken into account, it effectively reduces the coupled barrier energy in total, then the fusion cross sections (solid line) are in agreement with the experimental data in Fig.3. Meanwhile, we extract the barrier distributions for the ^{16}O+^{208}Pb system through comparison of the above fusion cross sections with the experimental data. It is shown in

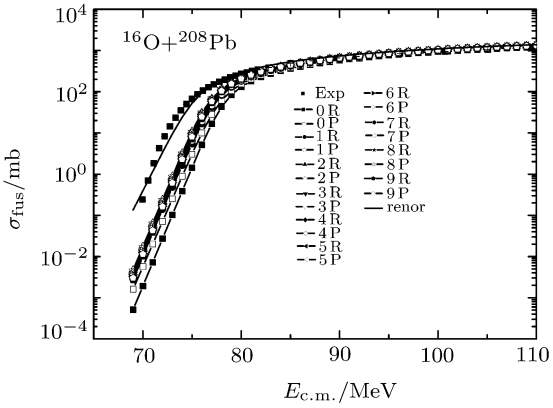


Fig.3. The calculated fusion cross sections for the ^{16}O+^{208}Pb system at different NN interactions on the basis of M3Y–Reid (full) and M3Y–Paris (open) interactions in comparison with the experimental data in Ref.[18]. The solid line denotes the result after the renormalization of the nuclear potential.

Fig.4 that the density-independent NN interactions result in the barriers moving to the highest position, and the density-dependent NN interactions give the similar barrier distributions. If the potential renormalization is considered, the barrier positions are nearly equal to those measured experimentally.

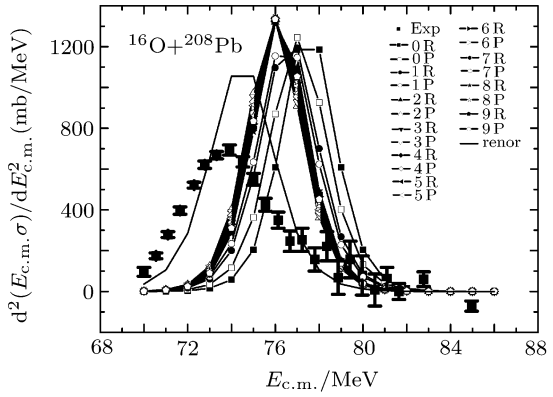


Fig.4. The extracted barrier distributions for the ^{16}O+^{208}Pb system at different NN interactions on the basis of M3Y–Reid (full) and M3Y–Paris (open) interactions in comparison with the experimental data in Ref.[18]. The solid line denotes the result after the renormalization of the nuclear potential.

In conclusion, we have calculated the folding nuclear potentials and Coulomb potentials for two spherical colliding nuclei ^{16}O and ^{208}Pb. The NN interactions include the density-independent M3Y–Reid and M3Y–Paris NN interactions with zero-range and finite-range exchange parts, and the density-dependent NN interactions with finite-range exchange part. The barrier energy for the M3Y–Reid interaction with zero-range exchange part is the largest, moreover, the barrier radius and curvature change remarkably in comparison with the other NN interactions. This set of parameters of the M3Y interaction fails to reproduce saturation property of cold nuclear matter. So it gives the smallest fusion cross sections. The density-dependent NN interactions which reproduce the basic properties of nuclear matter give the similar barrier energies, barrier radii and barrier curvatures. They show the similar fusion cross sections and the barrier distributions. For barrier distribution the density-independent NN interactions result in the barriers moving to the highest position. We renormalize the potential barrier due to coupling to the collective states of projectile and target at higher excitation energy. If the coupled-channel effect on the fusion barrier energy is considered, the fusion barrier is typically reduced by several percent. The calculated fusion cross sections and the barrier distributions are consistent with the corresponding experimental data. We hope the present studies may provide a good reference for the fusion calculations at energies near and below the Coulomb barrier.

References

[1] Goldberg D A, Smith S M, Pugh H G, Roos P G and Waal N S 1973 *Phys. Rev.* C **7** 1938

[2] Goldberg D A, Smith S M and Burdzik G F 1974 *Phys. Rev.* C **10** 1362

[3] Bohlen H G, Clover M R, Ingold G, Lettau H and Oertzen von W 1982 *Z. Phys.* A **308** 121

[4] Stiliarid E, Bohlen H G, Frobrich P, Gebauer B, Kolbert D, Oertzen von W, Wilpert M and Wilpert Th 1989 *Phys. Lett.* B **223** 291

[5] Zhang G L, Zhang H Q, Liu Z H, Zhang, C L, Lin, C J, Yang F, An, G P, Jia, H M, Wu Z D, Xu X X, Bai C L and Yu N 2007 *High. Energy. Phys. Nucl. Phys.* **31** 634

[6] Khoa Dao T and Satchler G R 2000 *Nucl. Phys.* A **668** 3

[7] Ma Y Q and Ma Z Y 2008 *Acta Phys. Sin.* **57** 74 (in Chinese)

[8] Vries De H, De Jager C W and De Vries C 1987 *At. Data Nucl. Data Tables* **36** 495

[9] Bertsch G, Borysowicz J, Mcmanus H and Ae W G 1977 *Nucl. Phys.* A **284** 399

[10] Anantaraman N, Toki H and Bertsch G F 1983 *Nucl. Phys.* A **398** 269

[11] Satchler G R and Love W G 1979 *Phys. Rep.* **55** 183

[12] Khoa D T and Oertzen von W 1993 *Phys. Lett.* B **304** 8

[13] Khoa D T, Satchler G R and von Oertzen W 1997 *Phys. Rev.* C **56** 954

[14] Brandan M E and Satchler G R 1997 *Phys. Rep.* C **285** 143

[15] Chamon L C, Nobre G P A, Pereira D, Rossi E S, Silva C P, Gasques L R and Carlson B V 2004 *Phys. Rev.* C **70** 014604

[16] Kemble E C 1935 *Phys. Rev.* **48** 549

[17] Hill D L and Wheeler J A 1953 *Phys. Rev.* **89** 1102

[18] Morton C R, Berriman A C, Dasgupta M, Hinde D J, Newton J O, Hagino K and Thompson I J 1999 *Phys. Rev.* C **60** 044608